Modeling resistance of colorectal peritoneal metastases to immune checkpoint blockade in humanized mice

Emre Küçükköse [iD],[1] Balthasar A Heesters [iD],[2] Julien Villaudy,[3,4] André Verheem,[1] Madalina Cercel,[4] Susan van Hal,[4] Sylvia F Boj,[5] Inne H M Borel Rinkes,[1] Cornelis J A Punt,[6] Jeanine M L Roodhart,[1,7] Jamila Laoukili,[1] Miriam Koopman,[7] Hergen Spits,[4,8] Onno Kranenburg [iD] [1,9]

ABSTRACT

Background The immunogenic nature of metastatic colorectal cancer (CRC) with high microsatellite instability (MSI-H) underlies their responsiveness to immune checkpoint blockade (ICB). However, resistance to ICB is commonly observed, and is associated with the presence of peritoneal-metastases and ascites formation. The mechanisms underlying this site-specific benefit of ICB are unknown.

Methods We created a novel model for spontaneous multiorgan metastasis in MSI-H CRC tumors by transplanting patient-derived organoids (PDO) into the cecum of humanized mice. Anti-programmed cell death protein-1 (PD-1) and anti-cytotoxic T-lymphocytes-associated protein 4 (CTLA-4) ICB treatment effects were analyzed in relation to the immune context of primary tumors, liver metastases, and peritoneal metastases. Immune profiling was performed by immunohistochemistry, flow cytometry and single-cell RNA sequencing. The role of B cells was assessed by antibody-mediated depletion. Immunosuppressive cytokine levels (interleukin (IL)-10, transforming growth factor (TGF) b1, TGFb2, TGFb3) were determined in ascites and serum samples by ELISA.

Results PDO-initiated primary tumors spontaneously metastasized to the liver and the peritoneum. Peritoneal-metastasis formation was accompanied by the accumulation of ascites. ICB completely cleared liver metastases and reduced primary tumor mass but had no effect on peritoneal metastases. This mimics clinical observations. After therapy discontinuation, primary tumor masses progressively decreased, but peritoneal metastases displayed unabated growth. Therapy efficacy correlated with the formation of tertiary lymphoid structures (TLS)—containing B cells and juxtaposed T cells—and with expression of an interferon-γ signature together with the B cell chemoattractant CXCL13. B cell depletion prevented liver-metastasis clearance by anti-CTLA-4 treatment. Peritoneal metastases were devoid of B cells and TLS, while the T cells in these lesions displayed a dysfunctional phenotype. Ascites samples from patients with cancer with peritoneal metastases and from the mouse model contained significantly higher levels of IL-10, TGFb1, TGFb2 and TGFb3 than serum samples.

Conclusions By combining organoid and humanized mouse technologies, we present a novel model for

WHAT IS ALREADY KNOWN ON THIS TOPIC

⇒ Immune checkpoint blockade (ICB) has revolutionized the treatment of patients with microsatellite instable colorectal cancer with metastatic disease, producing durable responses that result in a significantly improved survival. Despite the success of ICB, therapy resistance is observed in approximately one-third of the patients and is associated with peritoneal involvement and ascites formation. Analysis of clinical samples has revealed a correlation between the presence of B cells and tertiary lymphoid structures (TLS) and benefit from ICB, but a model system and empirical evidence for a role of B cells in successful ICB is lacking.

WHAT THIS STUDY ADDS

⇒ We have developed a novel humanized mouse model in which the clinically observed organ site-dependent benefit of ICB is faithfully recapitulated. Using this model we provide empirical evidence for a critical role for B cells in ICB-induced clearance of primary tumors and liver metastases. In the same mice, peritoneal metastases were therapy-resistant and lacked B cells and TLS. We identified very high levels of immunosuppressive cytokines in ascites as a potential cause for the observed resistance of peritoneal metastases to ICB.

HOW THIS STUDY MIGHT AFFECT RESEARCH, PRACTICE OR POLICY

⇒ The generated model can now be used for studying response and resistance to ICB in a patient (-derived organoids)-specific manner. Future applications of the model will include comparative analysis of the (potentially differential) response of metastases residing in distinct organ sites to ICB (lungs, brain, bone, etc), in relation to the local immune context. Furthermore, the model allows the rational design and testing of ICB-sensitization strategies, including those stimulating TLS formation and/or (local) neutralization of immunosuppressive cytokines.

spontaneous multiorgan metastasis by MSI-H CRC, in which the clinically observed organ site-dependent benefit of ICB is recapitulated. Moreover, we provide empirical

evidence for a critical role for B cells in the generation of site-dependent antitumor immunity following anti-CTLA-4 treatment. High levels of immunosuppressive cytokines in ascites may underlie the observed resistance of peritoneal metastases to ICB.

INTRODUCTION

Approximately 15% of all colorectal cancers (CRC) are caused by silencing or mutational inactivation of genes involved in DNA mismatch repair (MMR). A deficient MMR system leads to the accumulation of insertion and deletion mutations (indels) which generates potentially immunogenic neoepitopes and changes in the length of microsatellite repeats, known as microsatellite instability (MSI). A high level of MSI (MSI-H) in early-stage CRC is associated with a good prognosis. However, distant metastasis formation is observed in a small group of patients with MSI-H tumors, accounting for 3–5% of all cases of metastatic CRC (mCRC).[1] These patients have a poor prognosis and reduced benefit from chemotherapy.[2][3] Recent clinical studies show that immune checkpoint blockade (ICB) with antibodies targeting programmed cell death protein-1 (PD-1) and cytotoxic T-lymphocytes-associated protein 4 (CTLA-4),[4] can elicit antitumor immune responses against MSI-H mCRC, resulting in durable clinical benefit.[5–9] Indeed, MSI-H status predicts sensitivity to ICB in CRC and other cancer types and is now used in clinical practice to select patients with cancer for such treatment.[10][11]

Multiple biomarkers of response to ICB therapy, including tumor mutational burden and expression of the cytokines CXCL13 and CXCL9, have recently been identified in a large pan-cancer analysis of ICB-treated patients.[12] CXCL13 is an attractant for B cells and T follicular helper cells, that is produced by exhausted tumor-reactive PD-1$^+$ T cell clones residing in tertiary lymphoid structures (TLS).[13] The presence of B cells and TLS in tumors are associated with the response to anti-PD-1 in sarcoma, melanoma, and renal cell carcinoma.[14–16] Whether B cells and TLS are also important for the response to ICB in patients with MSI-H CRC is unknown. However, CXCL13 marks T_H1-like cells specifically enriched in MSI-H CRC[17] but whether these T_H1 cells are involved in the response to ICB, and whether CXCL13 produced by these cells recruits B cells in MSI-H CRC is currently not known.

While ICB therapy has revolutionized the treatment of MSI-H mCRC, approximately half of the patients experience disease progression within 2 years after therapy initiation.[9] Recent evidence indicates that the presence of peritoneal metastases and consequent ascites formation is associated with resistance to ICB in CRC.[18][19] A comprehensive understanding of what determines response and resistance to ICB requires the generation of model systems in which the functional contribution of specific biomarkers—including B cells—can be empirically tested. Possibly, such contributions may be distinct between tumor types, patients, and specific checkpoint

inhibitors. Here, we established a series of patient-derived organoids (PDOs) from MSI-H mCRC tumors to generate spontaneous metastasis models in mice with or without a human immune system (HIS). HIS mice with PDO-initiated MSI-H mCRC were then used to model ICB therapy. Anti-PD-1 and anti-CTLA-4 strongly reduced the growth of primary tumors and liver metastases, but peritoneal metastases were refractory to ICB, as is observed in clinical practice. B cell influx and TLS formation were observed in ICB-responding primary tumors and liver metastases. However, ICB-refractory peritoneal metastases were devoid of B cells and TLS and were (locally) exposed to very high levels of immunosuppressive cytokines in ascites. Removal of B cells with a depleting anti-CD20 antibody prevented anti-CTLA-4-induced clearance of primary tumors and liver metastases.

METHODS

See online supplemental material 1 for full methods descriptions.

In vitro organoid culture

Generation of tumor organoid cultures (MmC2-4) cultures was performed according to Sato *et al.*[20] Tumor organoid MmC1 was obtained from the Hubrecht Organoid Technology foundation. In summary, tissue specimens were cut into small fragments, washed multiple times with ice-cold phosphate-buffered saline (PBS) (Sigma-Aldrich) and digested with Liberase TH research grade (Roche, 0.1 mg/mL) for 1 hour at 37°C, with shaking every 15 min. After washout of Liberase with PBS, tumor cells were collected by centrifugation (1500 RPM; 5 min) and embedded in ice-cold Matrigel (Corning), mixed with a basal culture medium in a 3:1 ratio. The basal culture medium consisted of Advanced Dulbecco's Modified Eagle Medium (DMEM)/F12 medium (Invitrogen), N-2-hydroxyethylpiperazine-N-2-ethane sulfonic acid (HEPES) buffer (Sigma-Aldrich, 1 mM), Penicillin/Streptomycin (Sigma-Aldrich, 1%), GlutaMAX (Life Technologies, 1×), R-Spondin conditioned medium (20%), Noggin conditioned medium (10%), B27 (Life Technologies, 1×), Nicotinamide (Sigma-Aldrich, 10 mM), Prostaglandin E2 (Sigma-Aldrich, 10 nM), Gastrin (Sigma-Aldrich, 10 nM), N-acetylcysteine (Sigma-Aldrich, 1.25 mM), A83-01 (Tocris, 500 nM), Epidermal growth factor (EGF) (Life Technologies, 50 ng/mL) and SB202190 (Life Technologies, 3 μM). For passaging, between 7 and 14 days after initial plating, the tumor organoids were dissociated with TrypLE Express (Gibco) for 5–10 min at 37 and replated in a prewarmed 6-well plate. Rho-associated kinase inhibitor Y-27632 (Sigma-Aldrich, 10 μM) was added to culture medium on plating for 2 days.

Animal experiments

Laboratory animal study protocols 614-01-07 and 16-795-2-08 were approved by Utrecht and Amsterdam University's Animal Welfare Body, the Animal Ethics Committee

and licensed by the Central Authority for Scientific Procedures on Animals (license number AVD115002016614 and AVD118002016795). All experiments were conducted in accordance with the Dutch Experiments on Animals Act, in line with European Directive 2010/63/EU and by licensed personnel.

In vivo tumor-forming potential of the MSI-H CRC organoids was assessed by subcutaneous (s.c.) injections of 5×10^5 cells (dissociated using TripLE Express, resuspended in Matrigel/medium ratio 1:1) in both flanks of *NOD.Cg-Prkdc^scid Il2rg^tm1Wjl/SzJ* (NSG) male mice, between 8 and 10 weeks of age. The s.c. tumors became visible in 14 days and before reaching the human endpoint (tumor volume 1500 mm^3), the mice were sacrificed by cervical dislocation.

HIS mice were generated using *NOD.Cg-Prkdc^scid Il2rg^t-m1Wjl/SzJ* (NSG) mice as previously described.[21] Shortly, newborn NSG mice (females and males) younger than 5 days received sublethal irradiation of 1 Gy using a Cs137 source and an intrahepatic injection with 5×10^4 CD34$^+$ CD38$^-$ lineage hematopoietic progenitor cells isolated from fetal liver. Fetal tissue for reconstitution of mice was received after obtaining informed consent from the mother and with prior approval by the Medical Ethical Committee of the Academic Medical Center of the University of Amsterdam.

To evaluate the spontaneous metastatic capacity of the MSI-H CRC organoids, we made use of the murine orthotopic cecum-implantation model.[22] In summary, day before implantation, tumor organoids were dissociated into single cells and 2.5×10^5 cells were plated in 10 µL drops of neutralized Rat Tail High Concentrated Type I Collagen (Corning, C3867). Organoids were allowed to recover overnight at 37°C, 5% (volume/volume) CO_2. NSG and HIS mice were treated with a s.c. dose of carprofen (5 mg/kg, Rimadyl) 30 min before surgery and were subsequently sedated by using isoflurane inhalation anesthesia (2% (volume/volume) isoflurane/O_2 mixture). The cecum was exteriorized through a midline abdominal incision and a single collagen drop containing organoids was surgically transplanted in the cecal submucosa. Carprofen was administrated in drinking water for 3 days and Baytril (125 µg, s.c. injection) was given two times per day for 5 days. The following antibodies (derived from the UMCU Pharmacy) were used for in vivo treatment: OPDIVO (anti-PD-1, ABF4176) YERVOY (anti-CTLA-4, ABL1104), and MabThera (anti-CD20, N7395).

RESULTS
Generation of organoid models for MSI-H mCRC
Organoid technology allows the generation of 'tumor avatars' in vitro, with indefinite growth potential and maintenance of the genetic, phenotypic, and functional features of the original tumors.[23 24] Here, we applied organoid technology to generate models for MSI-H mCRC using biopsies and resection specimens from patients with MSI-H mCRC (online supplemental table

1). We established four MSI-H mCRC (MmC) organoid cultures (figure 1A), which demonstrated exponential growth for prolonged periods of time (>15 passages) and retained tumor-initiating potential (online supplemental figure S1A,B). MmC-PDOs showed loss of expression of MMR proteins and/or MSI, confirming their MSI-H status (online supplemental figure S1C,D). Whole-genome sequencing revealed tumor mutational burden values typical for MSI-H CRC[25] (figure 1B) with enrichment of specific mutational signatures known to be caused by a deficient MMR system (figure 1C). MmC1-3 were derived from sporadic MSI-H tumors with mutations in *BRAF* (MmC1-2) or *ERBB3* (MmC3), which are known to be associated with MSI-H CRC. MmC4 was derived from a Lynch syndrome tumor caused by an inactivating mutation in *MSH2* with loss of MSH2/MSH6 expression[26 27] (figure 1D). Karyotype analysis revealed gains and losses of various chromosomes and chromosomal segments (figure 1E), in line with the notion that karyotype changes occur in both microsatellite stable and MSI-H CRC.[28]

Spontaneous multiorgan metastasis formation by organoid-initiated primary tumors in immunodeficient mice
We next explored whether MmC-PDOs had retained metastatic capacity. Collagen-embedded, luciferase-transduced PDOs were implanted into the cecum submucosa of mice using an orthotopic transplantation protocol[29] (figure 1F). Luciferase-expressing MmC1-3, but not MmC4, organoids formed invasive, actively growing 'primary' tumors at the implantation site. Moreover, bioluminescence imaging showed spontaneous formation of distant metastases in liver (MmC1, MmC2), lungs (MmC2, MmC3) and peritoneum (MmC1-3), after approximately 3 weeks (figure 1F and G). Mice displayed a rapid deterioration of general health parameters, including ascites formation. The humane endpoint was generally reached after 4–6 weeks. Mice transplanted with MmC2 or MmC3 specifically developed dyspnea, presumably caused by lung metastasis formation. MmC1 was derived from a liver metastasis and caused liver metastasis formation in mice. MmC3 was derived from a lymph node metastasis and caused lung metastases in mice. MmC2 was derived from a donor whose clinical history cannot be retraced and formed many small metastases throughout the liver and the lungs (figure 1H–K). The observation that all organoids formed peritoneal metastases is consistent with the fact that MSI-H tumors are over-represented in patients with peritoneal metastases.[2] The different patterns of metastasis in the different MmC models and their (partial) concordance with clinically observed metastasis patterns suggests that metastatic organotropism of the original tumor may be preserved in the MmC models.

Introduction of an HIS does not affect primary tumor growth and patterns of metastasis
In patients with CRC, distant metastases occur most frequently in the liver. Therefore, we selected MmC1 for
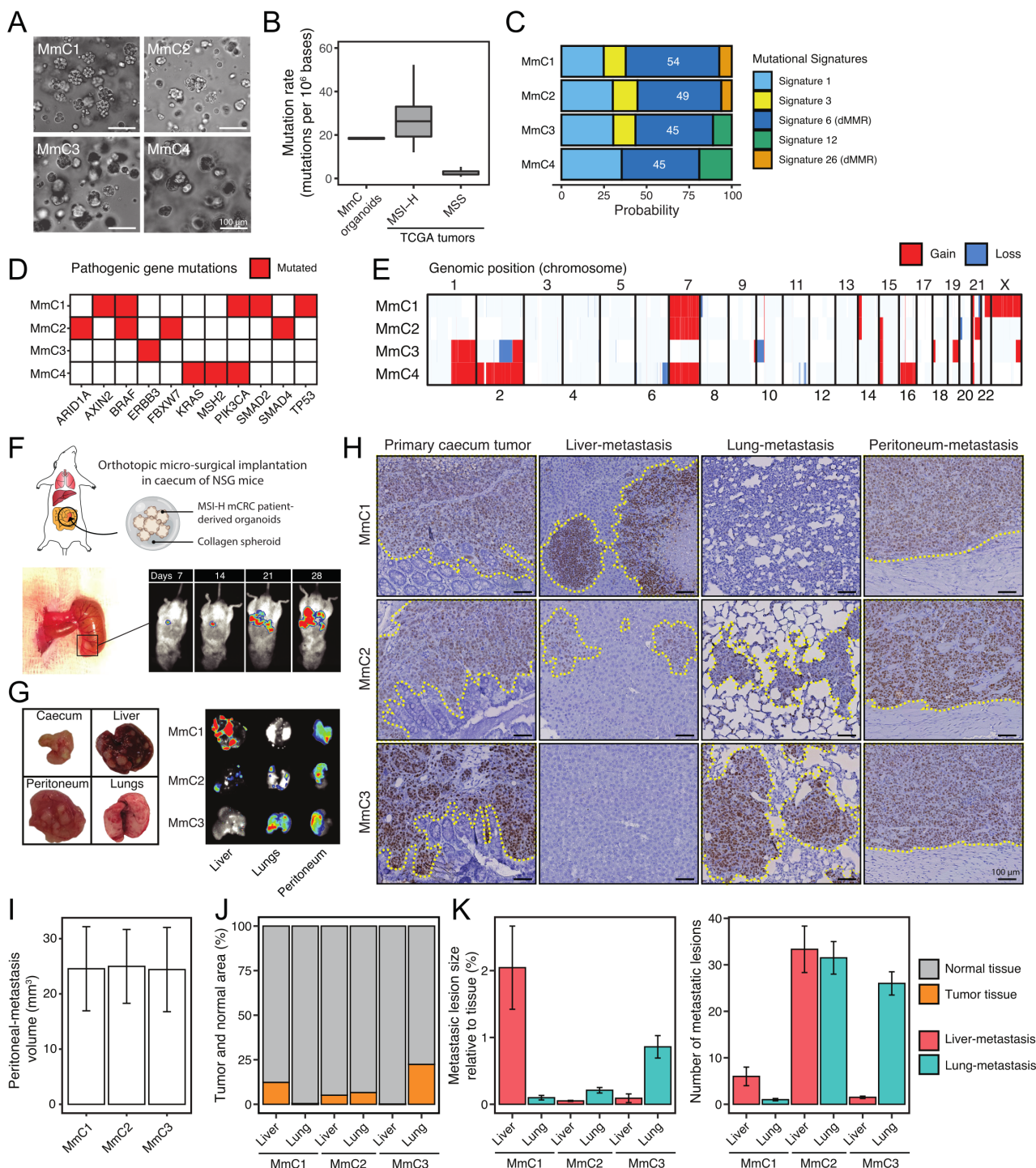
Figure 1 MmC organoids recapitulate genomic characteristics of MSI-H CRC tumors and retain metastatic capacity with patient-specific organ tropism. (A) Brightfield microscopic images of MmC-PDOs. (B) Tumor mutation burden (non-synonymous mutations/mb) in MmC-PDOs and MSS/MSI-H CRC tumors (TCGA). (C) Mutational signature probabilities in MmC-PDOs, determined by the nucleotide mutation types. (D) Mutation status of genes significantly mutated in MSI-H CRC according to TCGA. Red indicates mutated genes. (E) Copy number profile of MmC-PDOs for each chromosome. Gain (red) and loss (blue) in genomic position are indicated. (F) Schematic overview of MmC-PDO implantation under the cecum serosa-layer in NOD. Cg-*Prkdc^scid^Il2rg^tm1Wjl^*/SzJ (NSG) mice. Tumor/metastasis are monitored by using bioluminescence of luciferase-transduced MmC-PDOs. (G) Formation of primary tumor at cecum-implanted site and metastases in liver, peritoneum, and lungs in MmC1-3 models. (H) Histological hNucleoli staining of primary cecum tumor, liver metastasis, lung metastasis, and peritoneum metastasis for MmC1-3 models. Dashed yellow line indicates tumor/metastasis area. Scale-bar 100 µm. (I) Peritoneum-metastasis volume (mm³), (J) total metastases area relative to normal tissue, (K) number, and metastasis lesion size for MmC1-3 models (hNucleoli quantification). Three independent experiments, n=5 mice per experiment. CRC, colorectal cancer; mCRC, metastatic CRC; MSI-H, high level microsatellite instability; MSS, microsatellite stable; PDOs, patient-derived organoids; TCGA, The Cancer Genome Atlas.

further studies, aiming to model ICB therapy. To this end, MmC1 was transplanted into NSG mice with an HIS.[21] Successful humanization was assessed by determining the human immune cell engraftment score (>20%), and by analyzing human immune cell composition (online supplemental figure S2A). The presence of an HIS did not interfere with the formation or size of primary cecum tumors, nor with the formation of metastases in the liver or the peritoneum (figure 2A and B, online supplemental figure S2B). Thus, the tumors have induced immune tolerance in this model despite the major histocompatibility complex (MHC) mismatch with the human immune cells. To investigate the mechanism underlying the observed tolerance, we performed comparative gene expression analysis of MmC1 tumors growing in immune-deficient versus humanized mice by RNA sequencing (RNA-seq). The t-distributed stochastic neighbor embedding (t-SNE) algorithm separated tumors growing in either host (figure 2C). Gene ontology analysis of differentially expressed genes (n=213) demonstrated enrichment of signatures reflecting immune activation in tumors growing in HIS mice (figure 2D and E, online supplemental table 2). Tumor-reactive T cell populations can be identified in the circulation by high expression of PD-1.[13 30] Flow-cytometry analysis of blood samples revealed that the fraction of PD-1$^+$ cells within the circulating CD8$^+$ T cell population increased by 10-fold when all mice had developed extensive metastatic tumor growth (figure 2F). Examination of immune cell subset gene signatures[31] in the RNA-seq data, revealed high scores of 'T cell' and 'Cytotoxic T cell (CTL)' signatures in primary tumors and liver metastases but not in peritoneal metastases (figure 2G). Flow-cytometry analysis of fresh tumor tissue confirmed the high influx of T cells into primary tumor tissue, but not into peritoneal metastases (online supplemental figure S2C). Immunohistochemistry analysis on peritoneal metastases and matched primary tumors of two MSI-H patients confirmed that peritoneal metastases contain significantly lower numbers of infiltrated T cells than primary tumors (online supplemental figure S3). Tumors resist immune-mediated clearance by engaging immune checkpoints. Indeed, immune checkpoint ligand and receptor genes were highly expressed in primary tumors and liver metastases, but not in peritoneal metastases (figure 2H). Analysis of several large cohorts[25 32–34] of CRC tumors with available gene expression data also showed a strong correlation (Pearson's r=0.63 and p=3.3e-66) of the CTL signature with the immune checkpoint signature, suggesting immune checkpoints prevent infiltrating CTLs from attacking the tumors (online supplemental figure S4).

Analysis of the expression of 50 cancer hallmark gene signatures[35] showed that immune-related pathways (including interferon (IFN)-γ signaling) were expressed at higher levels in primary cecum tumors and in liver metastases than in peritoneal metastases (figure 2I), while transforming growth factor (TGF)β signaling was higher in peritoneal metastases. Of note, we recently demonstrated that human peritoneal metastases are characterized by a stroma-rich microenvironment and high TGFβ signaling,[36] which may lead to immune evasion.[37]

Together, the data reveal an important aspect of the nature of the PDO-HIS model. In general, three cancer-immune phenotypes can be recognized: inflamed, immune-desert, and immune-excluded.[38] The RNA-seq and immunohistochemistry data show that the tumors in the PDO-HIS model belong to the first category: immune cells infiltrate into the tumors, immune checkpoints are activated, while tumor growth is not abated.

ICB therapy reduces primary tumor size and eradicates liver metastases but has no effect on peritoneal metastases

To test the role of immune checkpoints in the induction of tolerance, we treated MmC1 tumor-bearing HIS mice with anti-PD-1 (nivolumab) or anti-CTLA-4 (ipilimumab) 17 days after tumor initiation (figure 3A, online supplemental figure S5). Mice received six doses of either antibody. At the humane endpoint of the first control animals, all mice were sacrificed. Histological analyses showed that anti-PD-1 and anti-CTLA-4 therapy reduced primary tumor size, and caused complete eradication of liver metastases, but had no effect on peritoneal metastases (figure 3B–E), Anti-human IgG immunohistochemistry showed that both therapeutic antibodies were present within and throughout the peritoneal metastases, suggesting that the lack of treatment efficacy was not due to poor drug distribution (online supplemental figure S6). Both anti-PD-1 and anti-CTLA-4 caused a significant increase in spleen weight, indicating immune activation (figure 3F). ICB therapy caused an increase in the number of tumor-infiltrating hCD45$^+$ cells into primary cecum tumors, into liver metastases, and into peritoneal metastases (figure 3G). Histological analysis of liver tissues showed clusters of hCD45$^+$ cells occasionally surrounded a few residual tumor cells, reflecting active therapy-induced eradication of liver metastases by human immune cells (figure 3D). Taken together, ICB therapy evoked an antitumor immune response that completely eradicated liver metastases, but had no effect on peritoneal metastases, despite a therapy-induced immune cell influx. These data also indicate that tolerance in tumor-bearing HIS mice is at least partly mediated by checkpoint activation.

Response to ICB treatment is associated with B cell influx and the formation of TLS

Multiple biomarkers that predict response to ICB treatment have been identified though molecular analysis of clinical tissue samples. These include expression signature reflecting a T cell inflamed IFN-γ response,[39] messenger RNA expression of cytokines CXCL13, CXCL9[12–16 39] and the formation of TLS.[40 41] We found that all these clinically validated biomarkers predicting response to ICB treatment were significantly lower in (therapy-refractory; figure 3E) peritoneal metastases than in liver metastases or primary tumors (figure 4A–C and online supplemental figure S7A,B). These data are consistent with the
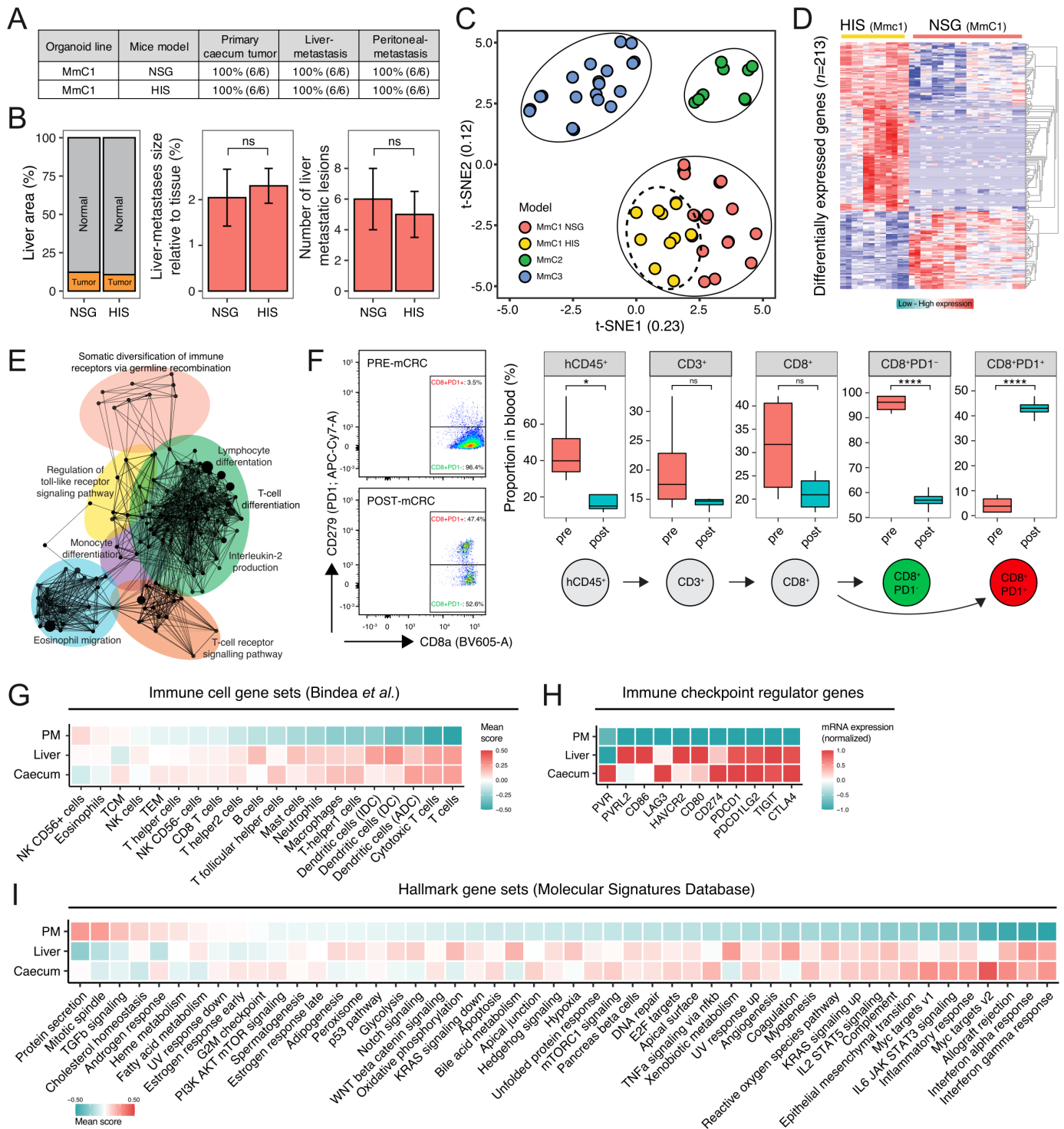
Figure 2 Preservation of metastasis patterns in humanized mice despite extensive influx of immune cells. (A) Comparison of NSG and HIS (humanized immune system) MmC1 mice models for tumor outgrowth and liver metastasis, and peritoneum metastasis, two independent experiments. (B) Histological quantification (hNucleoli) in NSG and HIS livers of MmC1 models, two independent experiments, n=6 mice per group. Mann-Whitney; ns, not significant. (C) t-SNE projection of RNA sequencing data of in vitro/vivo samples. (D) Differential gene expression analysis between NSG and HIS mice. Red indicates upregulated genes and blue vice versa. (E) Functionally grouped network with gene ontology terms as nodes of upregulated genes in HIS model (ClueGO Cytoscape). (F) Circulating immune populations in blood before/after implantation in HIS mice. Proportion of parent population shown (%). Mann-Whitney: *p<0.05; ****p<0.0001; ns, not significant. (G) Relative scores of immune cell gene sets,[31] (H) immune checkpoint regulator genes, and (I) hallmark gene sets, representing biological states or processes in RNA sequencing data of primary cecum tumor, liver metastases and peritoneum metastases derived from HIS mice samples. Color indicates expression: red=high; blue=low. HIS, human immune system; mCRC, metastatic colorectal cancer; PD-1, programmed cell death protein-1, t-SNE, t-distributed stochastic neighbor embedding.
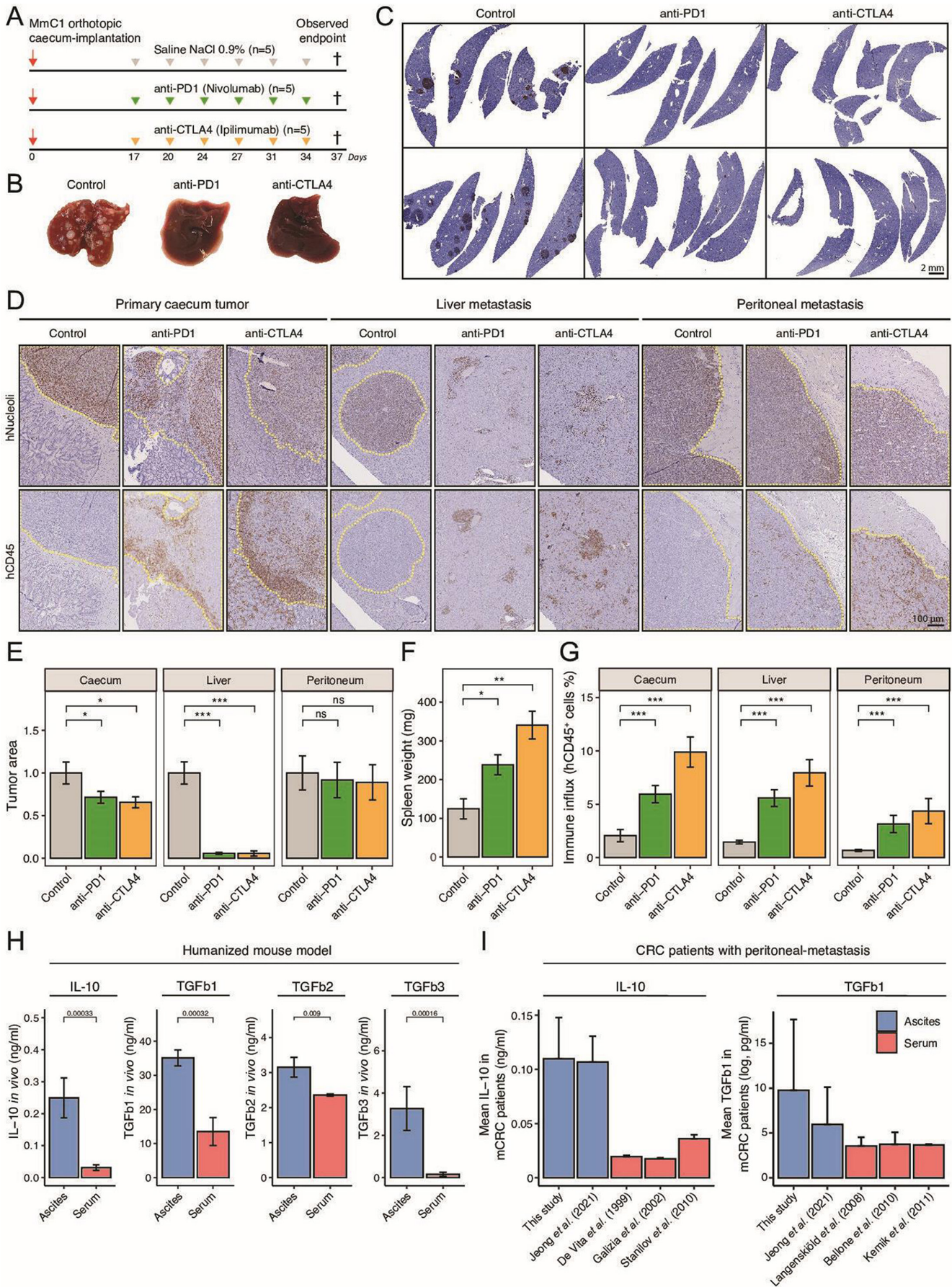
Figure 3 (Continued)

Figure 3 Eradication of liver metastasis but not peritoneal metastasis by ICB therapy. (A) Experimental protocol of treating HIS mice with anti-PD-1 (200 µg, i.p.) or anti-CTLA-4 (200 µg, i.p.), starting post 17 days orthotropic cecum-implantation. N=5 mice per group. All animals are sacrificed at the first observed endpoint of control mice. (B) Example livers of control, anti-PD-1-treated and anti-CTLA-4-treated mice at observed endpoint of control group. (C) Histological hNucleoli staining examples of liver sections from two different mice per group. Scale-bar is 2 mm (D) Histological hNucleoli (top) and hCD45 (bottom) staining of primary cecum tumor, liver metastasis, and peritoneum metastasis. Dashed yellow line indicates tumor/metastasis area. Scale-bar 100 µm. (E) Tumor/metastasis area (hNucleoli mm^2 in cecum, liver, and peritoneum. (F) Splenic weight (mg) at observed endpoint of control group, representative for degree of splenomegaly. (G) Total immune infiltration (hCD45% relative to tissue) in cecum, liver, and peritoneum. (H) Immune suppressive cytokine levels of IL-10, TGFb1, TGFb2 and TGFb3 in ascites versus serum samples of HIS mice. (I) Mean IL-10 and TGFb1 concentration in ascites or serum samples of human patients with metastatic CRC.[43–49] Data shown as mean±SEM. Mann-Whitney: *p<0.05; **p<0.01; ***p<0.001, ****p<0.0001; CRC, colorectal cancer; CTLA-4, cytotoxic T-lymphocytes-associated protein 4; HIS, human immune system; ICB, immune checkpoint blockade; IL, interleukin; i.p., intraperitoneal injection; mCRC, metastatic CRC; ns, not significant; PD-1, programmed death ligand-1; TGF, transforming growth factor.

observation that the presence of peritoneal metastases and ascites in patients with cancer is associated with therapy resistance.[18 19] In the models generated in this report, the development of peritoneal metastases is associated with the formation of ascites. This prompted us to compare the levels of several immunosuppressive cytokines (interleukin (IL)-10, TGFb1, TGFb2, TGFb3) in ascites (to which peritoneal metastases are exposed) versus those in serum (to which systemic metastases are exposed). The levels of all four cytokines were significantly higher (2–20-fold change) in ascites samples compared with serum samples from the same mice (figure 3H). Next, we analyzed ascites samples directly derived from patients with cancer with inoperable peritoneal metastases.[42] We found that the mean concentration of IL-10 and TGFb1 was significantly higher in ascites samples from this cohort, and from a previously published series,[43] than in the serum of patients with metastatic CRC[44–49] (figure 3I).

The presence of B cells in tumors is associated with the response to anti-PD-1 in various cancer types,[14–16] but its impact on ICB in patients with mCRC is currently unknown. To this end, we analyzed CD20$^+$ B cells found in peripheral blood, spleen, bone-marrow, primary tumor and liver tissues in control-treated and anti-CTLA-4-treated mice using antibodies against IgD, IgM and CD24 (online supplemental figure S7C). As expected, most B cells in bone marrow were CD24$^+$ IgD$^-$ IgM$^-$ pro B cells whereas in peripheral blood most B cells were CD24$^-$ IgD$^+$ IgM$^+$ naïve B cells. Treatment with anti-CTLA-4 resulted in an increase of CD24$^-$ IgD$^-$ IgM$^+$ B cells and CD24$^-$ IgD$^-$ IgM$^-$ B cells—which likely represent switched B cells—in the cecum but not in other compartments.

Besides the presence of B cells per se, their structural organization together with T cells in TLS predicts response to ICB.[14–16] Histological (hCD45) analysis on tissue sections of tumor-bearing anti-PD-1-treated and anti-CTLA-4-treated HIS mice showed extensive formation of TLS-like immune cell aggregates in the liver (figure 4A). In addition, these structures were also observed in the periphery of some of the primary tumors, but to a much lesser extent (figure 4B and C). The TLS-like structures were not observed in or around peritoneal metastases (figure 4C). TLS support B cell maturation and may serve as localized platforms for the generation of antitumor B

cell and T cell responses.[41] Histologically, TLS are characterized by distinct compartments of B cells, T cells, and macrophages.[41] Histological analysis showed the presence of TLS in the livers and around the primary cecum tumors of ICB-treated mice, consisting of a central region of CD20$^+$ B cells surrounded by CD8$^+$ T cells. The B cells were localized near CD8$^+$ T cells (figure 4A and B). CD68$^+$ macrophages were also present within these structures (figure 4A and B). Significant treatment-induced influx of hCD45$^+$ immune cells, including CD8$^+$ T cells, was observed in tumors growing at all sites, including peritoneal metastases (figures 3D–G and 4D). By contrast, ICB caused influx of B cells into primary cecum tumors and into liver metastases, but not into peritoneal metastases (figure 4E, online supplemental figure S7D). ICB had no significant effect on infiltration of FOXP3$^+$ regulatory T cells or CD68$^+$ macrophages into tumors growing at any of the three sites (figure 4F and G).

In the experiment presented in figure 4, all mice were sacrificed at the same time point to enable a comparative immune cell analysis in tumor tissue samples of the distinct groups. We noted that most animals in the treated groups had not reached the humane endpoint, which is usually caused by disease-related discomfort including ascites formation. Moreover, the primary tumors displayed an intermediate treatment response but did occasionally show TLS formation, suggesting that regression of the primary tumor bulk may take more time than regression of smaller liver metastases. To test this, mice were kept alive after ICB discontinuation, until they reached their individual humane endpoints. For this experiment, anti-CTLA-4 was chosen because it was more effective than anti-PD-1 in eliciting an antitumor immune response in this model. Two weeks after tumor initiation, one group of mice received control treatment, and two groups received anti-CTLA-4. The mice in one group receiving anti-CTLA-4 treatment (CTLA-4-group 1) were sacrificed at the same time as control mice, when these reached their humane endpoint. In the second treatment group, anti-CTLA-4 treatment was discontinued, after which each mouse was sacrificed at signs of discomfort (CTLA-4-group 2; figure 5A). Anti-CTLA-4 treatment significantly prolonged the survival of tumor-bearing mice in this group (figure 5B). Immunohistochemistry
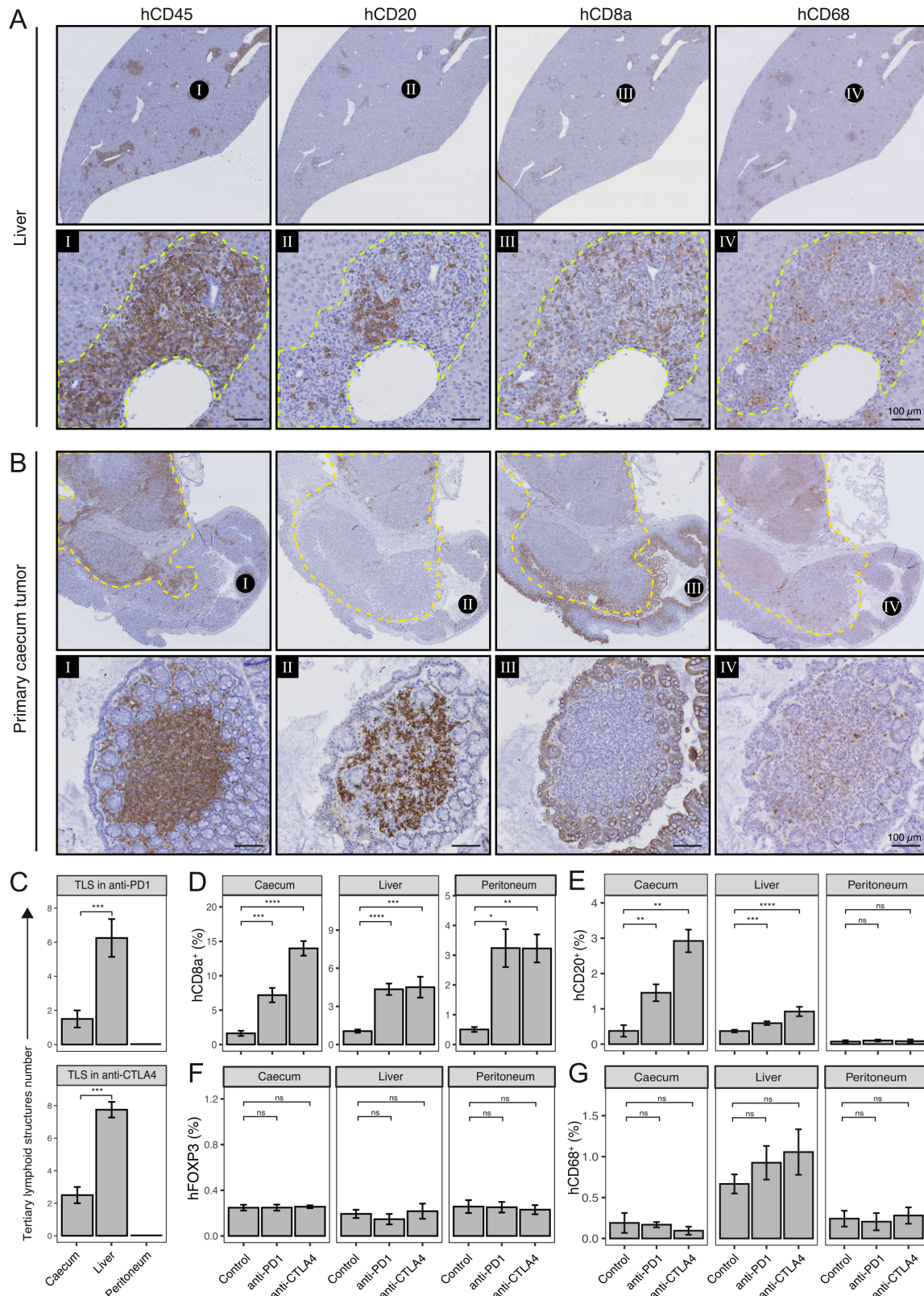
Figure 4 Immune checkpoint blockade induces formation of tertiary lymphoid structures (TLS) and distinct tumor-infiltrating lymphocytes (TIL) populations. (A) Histological examples of TLS in liver and (B) cecum of anti-CTLA-4-treated mouse. Spatial information of immune cells (hCD45), B cells (hCD20), Cytotoxic T cells (hCD8a) and macrophages (hCD68) in TLS are shown. Dashed yellow line indicates primary tumor. Scale-bar of area zoom 100 µm. (C) Number of TLS in cecum, liver, and peritoneum of anti-PD-1 (top) and anti-CTLA-4-treated mice (bottom). (D) Cytotoxic T cell (hCD8a), (E) B cell (hCD20), (F) regulatory T cells (hFOXP3), and (G) macrophages (hCD68) infiltration (% relative to tissue) in cecum, liver, and peritoneum. Mann-Whitney: *p<0.05; **p<0.01; ***p<0.001; ****p<0.0001; CTLA-4, cytotoxic T-lymphocytes-associated protein 4; ns, not significant; PD-1, programmed death ligand-1, TIL, tumor-infiltrating lymphocytes.
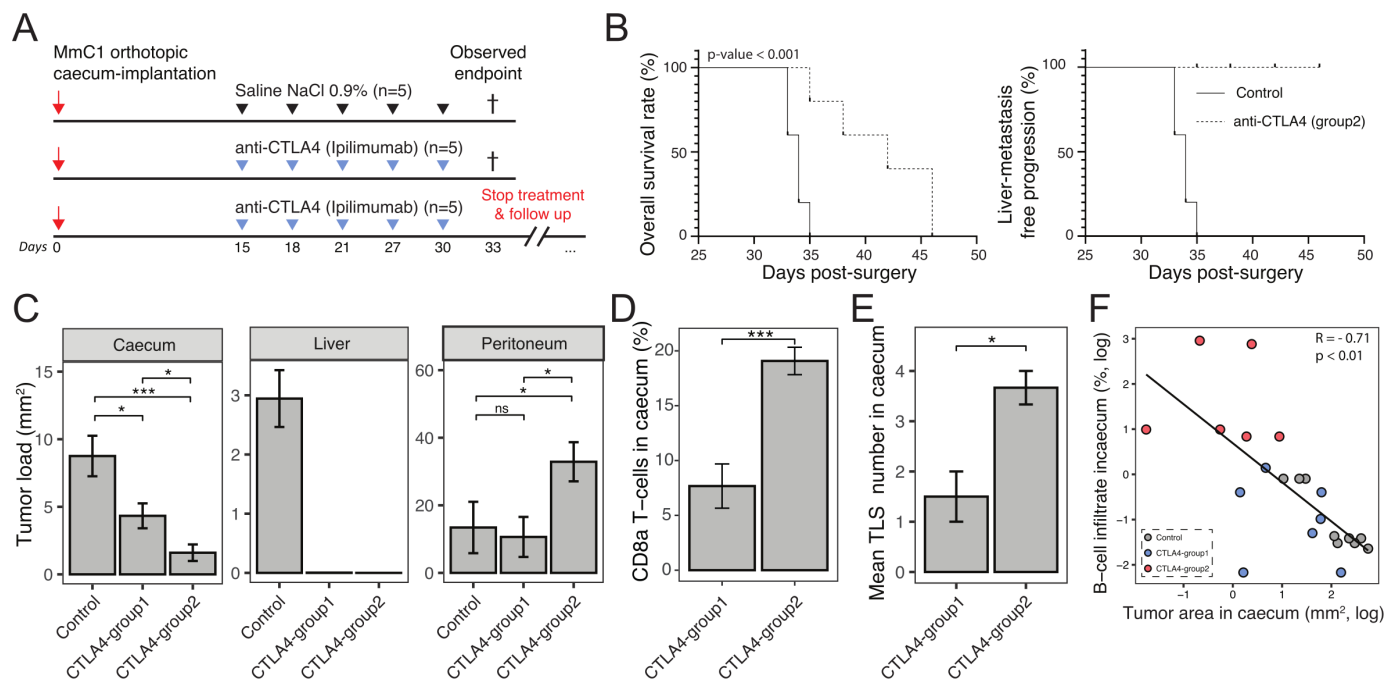
Figure 5 Extended period of life after anti-CTLA-4 therapy discontinuation leads to further antitumor response and is associated with B cell influx and TLS formation. (A) Experimental protocol of treating human immune system mice with anti-CTLA-4 (200 μg, i.p.), starting post 15 day's orthotropic cecum-implantation with 3 days interval. Inhibition with anti-CTLA-4 was discontinued at the observed endpoint (day 33) of the control group to monitor immune checkpoint blockade response. N=5 mice per group. (B) Kaplan-Meier: overall survival rate and liver metastasis-free progression. (C) Tumor/metastases area (hNuceloli mm^2 in cecum, liver, and peritoneum. (D) CD8a T cell infiltration in primary cecum tumor in CTLA-4-group 1 and CTLA-4-group 2 animals. (E) Number of TLS formation in cecum in CTLA-4-group 1 and CTLA-4-group 2 animals. Mann-Whitney: *p<0.05; **p<0.01; ***p<0.001; ****p<0.0001; ns, not significant. (F) Negative correlation with tumor area (mm^2) and B cell infiltrate (%) in cecum, log-scaled. Gray=control, blue=CTLA-4-group 1 and red=CTLA-4-group 2. CTLA-4, cytotoxic T-lymphocytes-associated protein 4; i.p., intraperitoneal injection; TLS, tertiary lymphoid structures.

using anti-human nucleoli for the detection of human tumor cells showed that the liver was completely tumor-free in all mice in both anti-CTLA-4 treatment groups. Moreover, primary tumor size was significantly smaller in CTLA-4-group 2 than in CTLA-4-group 1 (figure 5B,C) indicating that anti-CTLA-4 therapy resulted in ongoing primary tumor regression after therapy discontinuation.

The humane endpoint in CTLA-4-treated mice was determined by unabated growth of peritoneal metastases and associated discomfort, including ascites formation (figure 5C). Immunohistochemistry analysis of CTLA-4-treated primary tumors showed a significant increase of the influx of CD8a$^+$ T cells, B cells and increased TLS formation in mice in CTLA-group 2 when compared with CTLA-4-group 1. (figure 5D,E, online supplemental figure S8). Indeed, there was a highly significant correlation between B cell influx and tumor regression over time (figure 5F).

Depletion of B cells interferes with anti-CTLA-4-mediated eradication of liver metastases

The presence of TLS and B cells predicts the response of metastatic melanoma and sarcoma to immune checkpoint inhibitors.[14–16] However, empirical evidence for their contribution to treatment efficacy in these and other cancer types is currently lacking. To assess the

contribution of B cells to the observed eradication of liver metastases by ICB in our model, we made use of a B cell-depleting antibody (anti-CD20; rituximab) (figure 6A). Two weeks after tumor initiation in HIS mice, mice received either control treatment, anti-CTLA-4, anti-CD20 or anti-CTLA-4 and anti-CD20. All mice were sacrificed at the humane endpoint of the first control animals, allowing direct comparisons of tumor tissue. In the primary cecum tumors, B cells were localized within TLS and outside TLS at the tumor border (online supplemental figure S9). However, in liver metastases, B cells were mostly localized within TLS. More than 10-fold fewer B cells were observed in peritoneal metastases compared with either primary tumors or liver metastases (figure 6B). Following treatment with anti-CD20, B cells were depleted from primary tumors, liver metastases, peritoneal metastases, spleens, and bone marrow (figure 6B, online supplemental figure S9). B cell depletion prevented the regression of liver metastases by anti-CTLA-4 therapy. By contrast, the formation of peritoneal metastases was unaffected by B cell depletion, anti-CTLA-4-therapy or the combination-therapy (figure 6C,D). The extent of liver metastasis formation in mice receiving both anti-CD20 and anti-CTLA-4 was similar to that in mice receiving anti-CD20 alone. Flow cytometry analysis
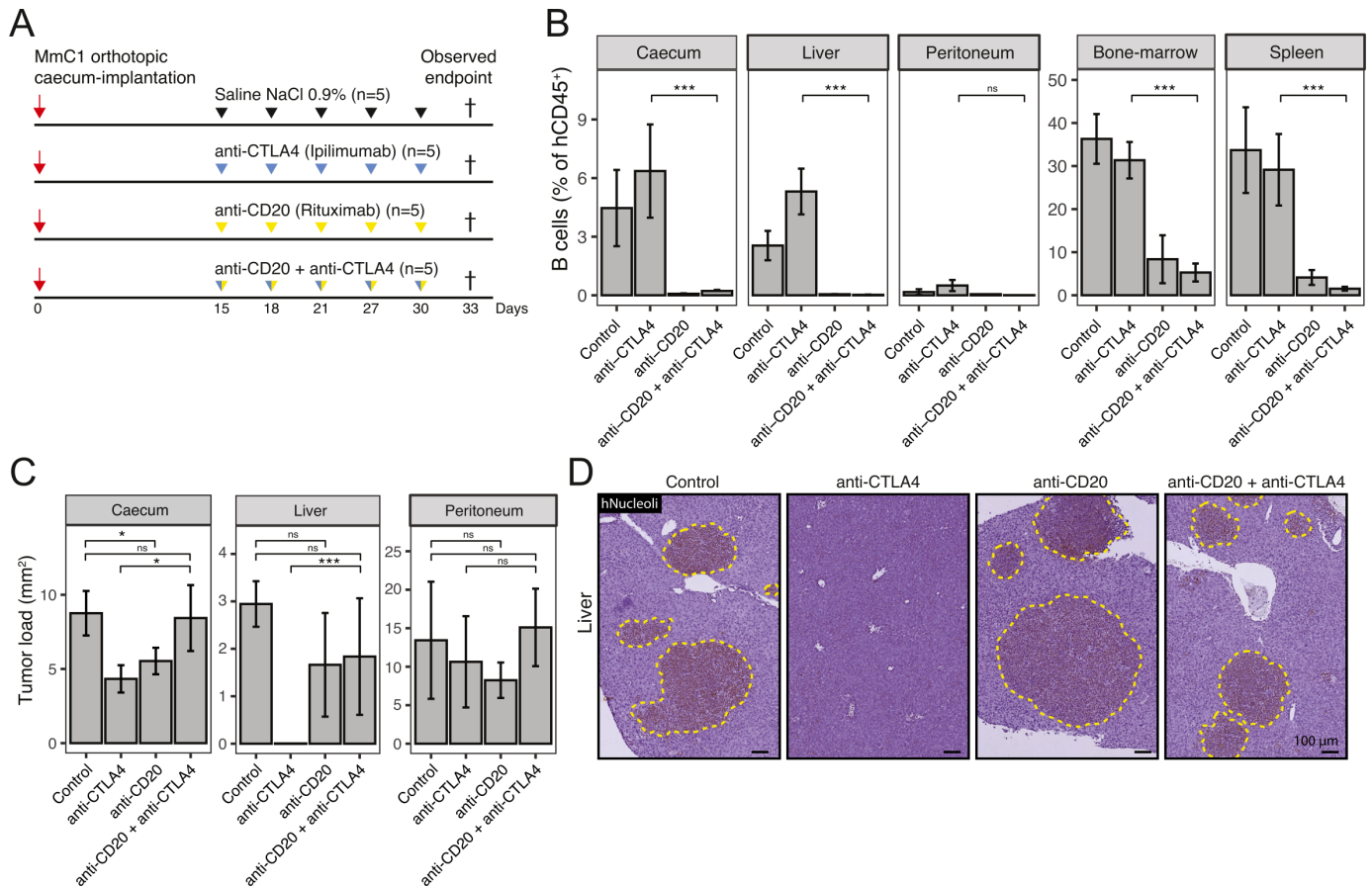
Figure 6 Depletion of B cells results in a significant decrease of antitumor response in anti-CTLA-4 treatment. (A) Experimental protocol of treating human immune system mice with anti-CTLA-4 (200 µg, i.p.), anti-CD20 (300 µg, i.p.) or combination, starting post 15 days orthotropic cecum-implantation with 3 days interval. N=5 mice per group. All animals are sacrificed at the first observed endpoint (t=33 days) of control mice. (B) B cell (hCD20) population (percentage of hCD45$^+$ cells) in cecum, liver, peritoneum, bone-marrow, and spleen samples, determined by flow cytometry. (C) Tumor/metastases area (hNucleoli mm^2 in cecum, liver, and peritoneum. Mann-Whitney: *p<0.05; **p<0.01; ***p<0.001; ****p<0.0001; ns, not significant. (D) Histological (hNucleoli) examples of liver metastases, scale-bar is 100 µm. CTLA-4, cytotoxic T-lymphocytes-associated protein 4; i.p., intraperitoneal.

revealed that B cell depletion (anti-CD20 and anti-CD20/antti-CTLA-4 treatment groups) reduced the proportion of CD45RO$^+$, CD69$^+$, and CCR7$^+$ CD8$^+$ T cells in the liver, when compared with mice treated with anti-CTLA-4 alone (online supplemental figure S10). Thus, B cells play an essential role in liver metastasis clearance by anti-CTLA-4. B cell depletion did not clearly influence the effect of anti-CTLA-4 on primary tumors but the formation of TLS in and around primary tumors was limited at the time of sacrifice (figure 6C). Of note, we found that B cell depletion alone had an inhibitory effect on the formation of primary tumors and liver metastases per se, pointing to a potential tumor-promoting function of B cells in the absence of ICB.

Anti-CTLA-4 induces site-specific transcriptional reprogramming of T cells and B cells

The above results demonstrate an essential role for B cells in establishing an effective antitumor immune response in the liver. Moreover, their relative absence from peritoneal metastases was associated with a lack of response to therapy. However, we did observe a treatment-induced influx of T cells into peritoneal metastases (figure 4D). This prompted us to analyze therapy-induced changes in T cell states in liver metastases versus peritoneal metastases. To this end, we performed single-cell RNA-seq on hCD45$^+$ immune cells isolated from both sites (figure 7A,B). Analysis of the expression of tumor-associated T cell signatures reflecting a cytotoxic versus a dysfunctional state[50] revealed that liver-derived T cells were predominantly cytotoxic, while peritoneal metastasis-derived T cells were largely dysfunctional. Indeed, expression of transcription factors marking cytotoxic (*KLF2*), or dysfunctional (*RBPJ*) T cells was significantly higher in liver metastasis and peritoneal metastasis derived T cells, respectively (figure 7C). The cytotoxic scores in T cells derived from the livers of control versus anti-CTLA-4-treated mice were not significantly different (online supplemental figure S11). However, the dysfunctional scores in T cells derived from peritoneal metastases were significantly higher in anti-CTLA-4-treated
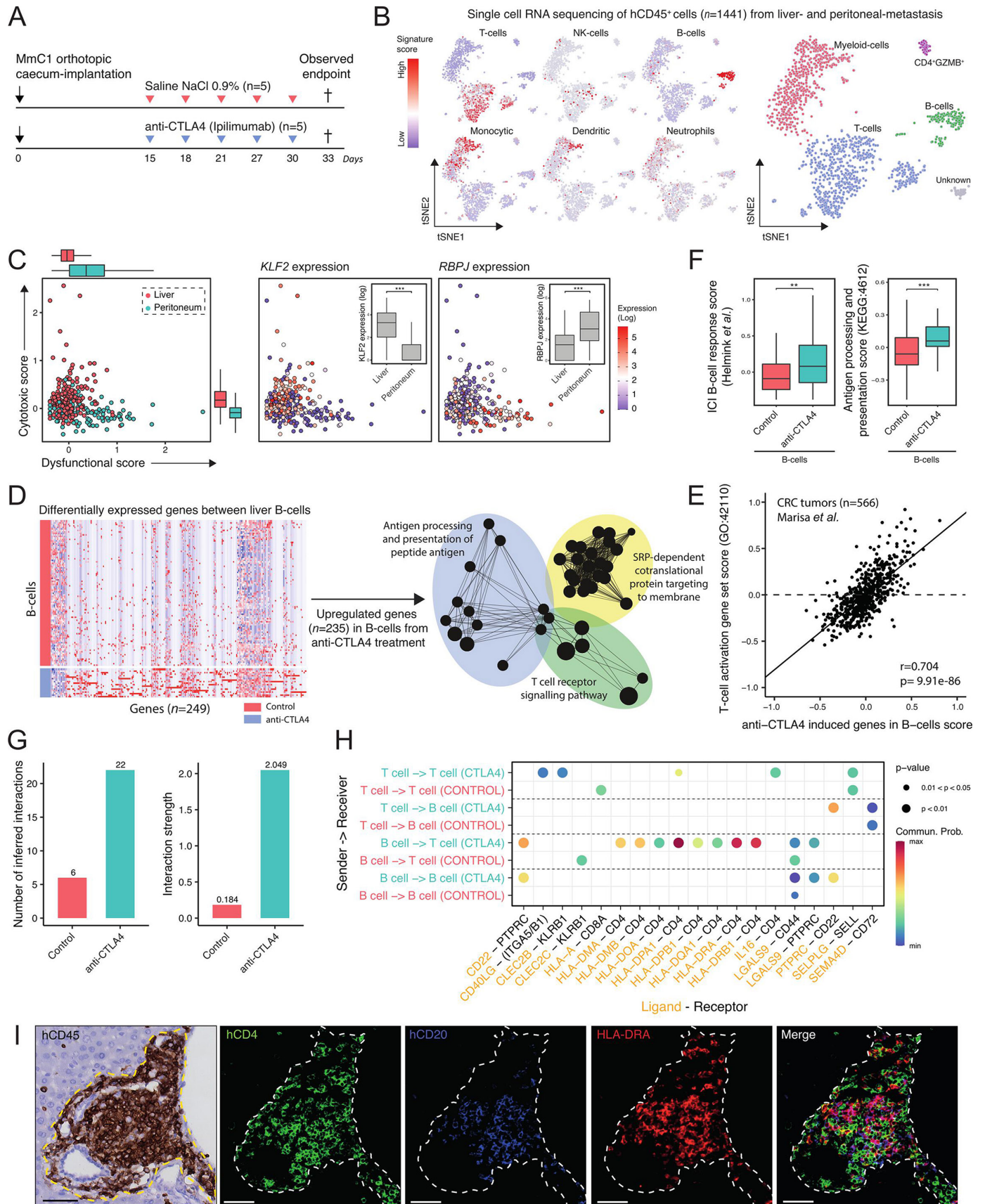
Figure 7 Immune checkpoint blockade induces site-specific transcriptional reprogramming in T cells and the formation of antigen-presenting B cells in TLS. (A) Experimental protocol of treating human immune system mice with anti-CTLA-4 (200 µg, i.p.), starting post 15 day's orthotropic cecum-implantation with 3 days interval. All animals are sacrificed at the first observed

Figure 7 (Continued)

endpoint (t=33 days) of control mice. Immune cells (hCD45^{+}) from liver metastasis and peritoneum metastasis were sorted for single-cell RNA sequencing. i.p. intraperitoneal injection. (B) t-SNE projection of single-cell RNA sequencing log-transformed counts on all detectable genes in hCD45^{+} cells. Scores of microenvironment cell populations[10], including cell types: T cell, NK cell, B cell, monocytic, dendritic and neutrophil. (C) Cytotoxic-scores and dysfunctional-scores[50] for T cells of liver (red) and peritoneum (blue) tissue. Expression (log) of associated transcription-factors *KLF2* and *RBPJ* with cytotoxic- and dysfunctional-scores, respectively. Mann-Whitney: **p<0.01; ***p<0.001. (D) Differential gene expression analysis between B cells from control and anti-CTLA-4-treated mice. Red and blue colors indicate upregulated and downregulated genes, respectively. Functional network analysis using ClueGO Cytoscape and gene ontology terms as nodes of upregulated genes (n=235) in anti-CTLA-4-treated derived B cells. (E) Positive correlation with anti-CTLA-4 induced genes in B cells signature and 'T cell activation' signature in a CRC cohort.[32] (F) Boxplots showing expression of a B cell gene signature associated with response to ICB therapy, and genes in the 'antigen processing and presentation' pathway (KEGG: hsa04612) in B cells in control and anti-CTLA-4-treated mice. (G) Inference and analysis of cell–cell communication using CellChat.[51] Bar plot represents the total number of inferred interactions (left) and interaction strength (right) of B and T cells derived from livers of control (red) or anti-CTLA-4 treated (blue) mice. (H) Bubble plot representing the communication probabilities for the identified ligand-receptor interactions between cell groups. (I) Histological analysis of HLA-DRA^{+} B cells juxtaposed to CD4^{+} T cells in TLS in anti-CTLA-4-treated mouse livers. Scale-bar 50 µm. CRC, colorectal cancer; CTLA-4, cytotoxic T-lymphocytes-associated protein 4; ICB, immune checkpoint blockade; i.p., intraperitoneal; NK, natural killer; TLS, tertiary lymphoid structures, t-SNE, t-distributed stochastic neighbor embedding.

mice when compared with control mice (online supplemental figure S11).

To investigate how B cells in TLS influence T cell function and T cell-mediated antitumor immunity, we assessed the impact of anti-CTLA-4 treatment on B cell states, using single-cell RNA-seq. Differential gene expression analysis showed that 235 genes were upregulated in B cells from anti-CTLA-4-treated mice when compared with B cells from control-treated mice, including MHC class II genes (*HLA-DRA, HLA-DRB5*) (figure 7D). There was no difference in the expression of genes encoding immunoglobulin heavy or light chains. Gene ontology analysis of the upregulated genes in anti-CTLA-4 treated B cells demonstrated enrichment of signatures reflecting 'antigen processing and presentation' as well as 'T cell receptor signalling' (figure 7D, online supplemental table 3). Indeed, expression of the anti-CTLA-4-induced B cell genes correlated extremely well with expression of the gene ontology term 'T cell activation (GO:42110)' in transcriptome data of CRC tumors[32] (Pearson r=0.70, p=9.9e-86; figure 7E). Furthermore, a B cell signature that predicts clinical responsiveness to ICB therapy in melanoma[14] was significantly higher in B cells from anti-CTLA-4-treated mice (figure 7F).

Next, we analyzed the communication between T cells and B cells in the livers from control and anti-CTLA-4-treated mice using CellChat software.[51] We found that anti-CTLA-4 treatment significantly induced 22 interactions between liver-derived B cells and T cells, while only 6 such interactions were found in control mice (figure 7G). Of the 22 cell–cell interactions in anti-CTLA-4-treated mice, the vast majority (n=8) were HLA molecules expressed on B cells interacting with CD4 expressed on T cells, further supporting the notion that antigen presentation by B cells to CD4^{+} T cells is a potential mechanism of action in the eradication of liver metastases by anti-CTLA-4 treatment in the PDO-HIS model (figure 7H, online supplemental figure S12). Moreover, we also observed a CTLA-4-induced interaction between T cell-expressed IL-16 acting on T cell CD4, pointing

to a T cell recruitment pathway evoked by anti-CTLA-4 treatment.[52] Indeed, immunohistochemistry and immunofluorescence analysis demonstrated the presence of HLA-DRA^{+} B cells near CD4^{+} and CD8^{+} T cells in liver-resident TLS of anti-CTLA-4-treated mice (figure 7I, online supplemental figure S13). CXCL13-producing cells were also clearly detected in the same TLS. In addition, we observed significantly higher expression of MHC class II genes in myeloid cells on anti-CTLA-4 treatment (online supplemental figure S14A). Differential gene expression analyses showed that 53 genes were upregulated in CD4^{+} T cells from anti-CTLA-4-treated mice when compared with CD4^{+} T cells from control-treated mice. Gene ontology analysis showed that these genes reflected 'immune response-activating signal transduction' and 'regulation of T cell activation' (online supplemental figure 14B). In summary, anti-CTLA-4 treatment induced transcriptional reprogramming of T cells and B cells.

DISCUSSION

In this study, we have established a novel model for MSI-H mCRC, based on a combination of organoid and humanized mouse technologies. The kinetics of organoid-initiated tumor growth and metastasis formation were not significantly different in immune-deficient versus humanized mice indicating that the HIS in these mice was tolerant towards the growing, presumably MHC-disparate, tumors. This tolerance was at least partly mediated by CTLA-4 and PD-1, since antibodies blocking these checkpoints overcame the observed tolerance in both the liver and the cecum. Regression of the primary cecum tumor continued after cessation of the treatment, indicating that once tolerance was broken by ICB therapy the effector immune cells continue to attack the tumor in the absence of the blocking antibodies. Whereas the primary tumor and liver metastases were eradicated by the ICB, peritoneal metastases were not affected, and tumor-bearing mice eventually succumbed to unabated growth of peritoneal metastases. CD8^{+} T cell influx was observed

in the primary tumor and liver metastases but less in the peritoneum. Moreover, CD8^{+} T cells in liver metastases were in an active cytotoxic state whereas those in the peritoneum were in a dysfunctional state. These observations are consistent with the generally accepted idea that active CD8^{+} CTL mediate tumor regression. Given the similarities regarding disease progression and response to ICB in patients with MSI-H cancer and the model presented in this report, the alloantigens in the model may be considered as surrogate neoantigens.

The differential site-specific response to anti-CTLA-4 treatment correlated with the presence of TLS and B cells. This is consistent with recent observations showing an association of the presence of TLS and B cells in tumors with a favorable outcome in patients treated with anti-PD-1.[14–16] An expression signature for memory B cells has also been correlated with response to anti-CTLA-4.[53] The PDO-HIS model presented here provides empirical evidence—through B cell depletion—of an essential role for B cells in the eradication of liver metastases by anti-CTLA-4 therapy. B cells may help generate an effective antitumor immune response via several mechanisms. We found that B cells in primary tumors and liver metastases express high levels of class II MHC antigens and are in close physical contact with CD4^{+} T cells within TLS, as has been observed in patient tissues[54] suggesting that the B cells activate CD4^{+} T cells which may subsequently help CD8^{+} CTL to attack tumor cells. Because the tumor cells are at least partly MHC disparate from the T cells and B cells, one should assume that the T cells are activated by an indirect alloantigen pathway.[55] B cells may also contribute to anti-CTLA-4-induced tumor regression by producing antibodies that may mediate complement-mediated cytotoxicity, or antibody-dependent-cellular cytotoxicity mediated by FcR-expressing effector cells such as natural killer cells and/or monocytes. A recent study in syngeneic mouse models for triple negative breast cancer showed that B cells and T cells activate each other during ICB with anti-CTLA-4 and anti-PD-1.[54] In this setting, the activated T follicular helper cells provided help to B cells to produce antibodies and loss of antibody secretion concomitant with ICB diminished the antitumor response.[54] We performed a limited analysis of the B cells present in the tumors, which suggested that only in the cecum a change in the B cell composition occurred. There was an increase in CD24^{−} IgM^{+} IgD^{−} and switched, CD24^{−} IgM^{−} IgD^{−} cells in the cecum after treatment with anti-CTLA-4, but whether this results in production of tumor-specific IgM/IgG/IgA antibodies has yet to be determined. B cells may also be important for formation of the intratumor TLS, thereby creating an environment for optimal interaction of T cells with B cells and dendritic cells. We found that B cells in cecum tumors and liver metastases expressed lymphotoxin alpha and beta transcripts, making it likely that they express $LT\alpha1\beta2$ on the cell surface. However, how TLS in these niches were formed in the absence of human non-hematopoietic stromal cells remains to be established.

Our finding that treatment benefit was dependent on the anatomical site where tumor cells were growing indicates that organ-specific niches are important determinants of treatment outcome. Organ site-dependent TLS formation has previously been demonstrated in mouse models of metastatic breast cancer.[56] Likewise, organ site-dependent differences in the response to ICB therapy have recently also been demonstrated in models for castration-resistant prostate cancer.[57] In the latter study, TGFβ signaling in the bone marrow niche prevented the generation of an effective immune response against bone metastases, and this could be relieved by TGFβ inhibition. Elucidating the influence of organ site on ICB therapy response is now recognized as an important novel area of research that is aimed at elucidating the mechanisms of resistance against ICB therapies.[4]

The finding that peritoneal metastases in this model are insensitive to ICB are clinically highly relevant, as recent studies have demonstrated that patients with MSI-H mCRC with peritoneal metastases and ascites are unlikely to benefit from ICB.[18 19] Moreover, our finding that ascites contains very high levels of immunosuppressive cytokines (both in patients with cancer and in the model) provides a first clue as to why peritoneal metastases may be refractory to ICB. Follow-up studies with specific antibodies or inhibitors neutralizing one or more of these immunosuppressive signals (including IL-10 and the various TGFβ isoforms) are needed to identify cause-effect relationships and design and test therapeutic approaches that may sensitize the poor-prognosis subgroup of patients with MSI-H mCRC with peritoneal metastases to ICB. Alternatively, the models can be applied to design TLS biogenesis-stimulating therapeutic approaches in the peritoneum, such as tumor vessel normalization.[58] Finally, by choosing specific PDOs with distinct patterns of metastatic organotropism the humanized mouse models provide a unique platform for studying organ site-specific responses to ICB. Possibly, distinct strategies will be needed to sensitize metastases growing in these completely distinct microenvironments, to ICB.

Author affiliations

[1]Laboratory Translational Oncology, Division of Imaging and Cancer, University Medical Center Utrecht, Utrecht, The Netherlands
[2]Pharmaceutical Sciences, Utrecht University Faculty of Science, Utrecht, The Netherlands
[3]J&S Preclinical Solutions, Oss, The Netherlands
[4]AIMM Therapeutics, Amsterdam, The Netherlands
[5]Hubrecht Organoid Technology, Utrecht, The Netherlands
[6]Julius Centre for Health Sciences and Primary Care, University Medical Center Utrecht, Utrecht, The Netherlands
[7]Department of Medical Oncology, University Medical Center Utrecht, Utrecht, The Netherlands
[8]Experimental Immunology, Amsterdam University Medical Centres, Amsterdam, The Netherlands
[9]Utrecht Platform for Organoid Technology, Utrecht University, Utrecht, The Netherlands

ORCID iDs
Emre Küçükköse http://orcid.org/0000-0002-8983-9464
Balthasar A Heesters http://orcid.org/0000-0002-2909-8481
Onno Kranenburg http://orcid.org/0000-0002-2112-4390

REFERENCES

1 Venderbosch S, Nagtegaal ID, Maughan TS, *et al*. Mismatch repair status and BRAF mutation status in metastatic colorectal cancer patients: a pooled analysis of the CAIRO, CAIRO2, COIN, and FOCUS studies. *Clin Cancer Res* 2014;20:5322–30.
2 Kim CG, Ahn JB, Jung M, *et al*. Effects of microsatellite instability on recurrence patterns and outcomes in colorectal cancers. *Br J Cancer* 2016;115:25–33.
3 Tran B, Kopetz S, Tie J, *et al*. Impact of BRAF mutation and microsatellite instability on the pattern of metastatic spread and prognosis in metastatic colorectal cancer. *Cancer* 2011;117:4623–32.
4 Sharma P, Allison JP. Dissecting the mechanisms of immune checkpoint therapy. *Nat Rev Immunol* 2020;20:75–6.
5 Chalabi M, Fanchi LF, Dijkstra KK, *et al*. Neoadjuvant immunotherapy leads to pathological responses in MMR-proficient and MMR-deficient early-stage colon cancers. *Nat Med* 2020;26:566–76.
6 Overman MJ, Lonardi S, Wong KYM, *et al*. Durable clinical benefit with nivolumab plus ipilimumab in DNA mismatch Repair-Deficient/Microsatellite Instability-High metastatic colorectal cancer. *J Clin Oncol* 2018;36:773–9.
7 Overman MJ, McDermott R, Leach JL, *et al*. Nivolumab in patients with metastatic DNA mismatch repair-deficient or microsatellite instability-high colorectal cancer (CheckMate 142): an open-label, multicentre, phase 2 study. *Lancet Oncol* 2017;18:1182–91.
8 Le DT, Uram JN, Wang H, *et al*. PD-1 blockade in tumors with mismatch-repair deficiency. *N Engl J Med* 2015;372:2509–20.
9 André T, Shiu K-K, Kim TW, *et al*. Pembrolizumab in Microsatellite-Instability-High advanced colorectal cancer. *N Engl J Med* 2020;383:2207–18.
10 Marisa L, Svrcek M, Collura A, *et al*. The balance between cytotoxic T-cell lymphocytes and immune checkpoint expression in the prognosis of colon tumors. *J Natl Cancer Inst* 2018;11010.1093/jnci/djx136. [Epub ahead of print: 01 01 2018].
11 Southey MC, Jenkins MA, Mead L, *et al*. Use of molecular tumor characteristics to prioritize mismatch repair gene testing in early-onset colorectal cancer. *J Clin Oncol* 2005;23:6524–32.
12 Litchfield K, Reading JL, Puttick C, *et al*. Meta-Analysis of tumor- and T cell-intrinsic mechanisms of sensitization to checkpoint inhibition. *Cell* 2021;184:e14:596–614.
13 Thommen DS, Koelzer VH, Herzig P, *et al*. A transcriptionally and functionally distinct PD-1⁺ CD8⁺ T cell pool with predictive potential in non-small-cell lung cancer treated with PD-1 blockade. *Nat Med* 2018;24:994–1004.
14 Helmink BA, Reddy SM, Gao J, *et al*. B cells and tertiary lymphoid structures promote immunotherapy response. *Nature* 2020;577:549–55.
15 Cabrita R, Lauss M, Sanna A, *et al*. Tertiary lymphoid structures improve immunotherapy and survival in melanoma. *Nature* 2020;577:561–5.
16 Petitprez F, de Reyniès A, Keung EZ, *et al*. B cells are associated with survival and immunotherapy response in sarcoma. *Nature* 2020;577:556–60.
17 Zhang L, Yu X, Zheng L, *et al*. Lineage tracking reveals dynamic relationships of T cells in colorectal cancer. *Nature* 2018;564:268–72.
18 Chow A, Schad S, Green MD, *et al*. Tim-4+ cavity-resident macrophages impair anti-tumor CD8+ T cell immunity. *Cancer Cell* 2021;39:973–88.
19 Fucà G, Cohen R, Lonardi S, *et al*. Ascites and resistance to immune checkpoint inhibition in dMMR/MSI-H metastatic colorectal and gastric cancers. *J Immunother Cancer* 2022;10:e004001.
20 Sato T, Stange DE, Ferrante M, *et al*. Long-Term expansion of epithelial organoids from human colon, adenoma, adenocarcinoma, and Barrett's epithelium. *Gastroenterology* 2011;141:1762–72.
21 Legrand N, Weijer K, Spits H. Experimental model for the study of the human immune system: production and monitoring of "human immune system" Rag2-/-gamma c-/- mice. *Methods Mol Biol* 2008;415:65–82.
22 Fumagalli A, Suijkerbuijk SJE, Begthel H, *et al*. A surgical orthotopic organoid transplantation approach in mice to visualize and study colorectal cancer progression. *Nat Protoc* 2018;13:235–47.
23 van de Wetering M, Francies HE, Francis JM, *et al*. Prospective derivation of a living organoid Biobank of colorectal cancer patients. *Cell* 2015;161:933–45.
24 Fujii M, Shimokawa M, Date S, *et al*. A colorectal tumor organoid library demonstrates progressive loss of niche factor requirements during tumorigenesis. *Cell Stem Cell* 2016;18:827–38.
25 Cancer Genome Atlas Network. Comprehensive molecular characterization of human colon and rectal cancer. *Nature* 2012;487:330–7.
26 Loree JM, Bailey AM, Johnson AM, *et al*. Molecular landscape of ErbB2/ErbB3 mutated colorectal cancer. *J Natl Cancer Inst* 2018;110:1409–17.
27 Thiel A, Ristimäki A. Toward a molecular classification of colorectal cancer: the role of BRAF. *Front Oncol* 2013;3:281.
28 Bolhaqueiro ACF, Ponsioen B, Bakker B, *et al*. Ongoing chromosomal instability and karyotype evolution in human colorectal cancer organoids. *Nat Genet* 2019;51:824–34.
29 Fumagalli A, Drost J, Suijkerbuijk SJE, *et al*. Genetic dissection of colorectal cancer progression by orthotopic transplantation

of engineered cancer organoids. *Proc Natl Acad Sci U S A* 2017;114:E2357–64.

30 Gros A, Parkhurst MR, Tran E, *et al*. Prospective identification of neoantigen-specific lymphocytes in the peripheral blood of melanoma patients. *Nat Med* 2016;22:433–8.

31 Bindea G, Mlecnik B, Tosolini M, *et al*. Spatiotemporal dynamics of intratumoral immune cells reveal the immune landscape in human cancer. *Immunity* 2013;39:782–95.

32 Marisa L, de Reyniès A, Duval A, *et al*. Gene expression classification of colon cancer into molecular subtypes: characterization, validation, and prognostic value. *PLoS Med* 2013;10:e1001453.

33 de Sousa E Melo F, Colak S, Buikhuisen J, *et al*. Methylation of cancer-stem-cell-associated Wnt target genes predicts poor prognosis in colorectal cancer patients. *Cell Stem Cell* 2011;9:476–85.

34 De Sousa E Melo F, Wang X, Jansen M, *et al*. Poor-Prognosis colon cancer is defined by a molecularly distinct subtype and develops from serrated precursor lesions. *Nat Med* 2013;19:614–8.

35 Liberzon A, Birger C, Thorvaldsdóttir H, *et al*. The molecular signatures database (MSigDB) hallmark gene set collection. *Cell Syst* 2015;1:417–25.

36 Laoukili J, Constantinides A, Wassenaar ECE, *et al*. Peritoneal metastases from colorectal cancer belong to consensus molecular subtype 4 and are sensitised to oxaliplatin by inhibiting reducing capacity. *Br J Cancer* 2022;126:1824–33.

37 Tauriello DVF, Palomo-Ponce S, Stork D, *et al*. TGFbeta drives immune evasion in genetically reconstituted colon cancer metastasis. *Nature* 2018;554:538–43.

38 Chen DS, Mellman I. Elements of cancer immunity and the cancer-immune set point. *Nature* 2017;541:321–30.

39 Ayers M, Lunceford J, Nebozhyn M, *et al*. IFN-γ-related mRNA profile predicts clinical response to PD-1 blockade. *J Clin Invest* 2017;127:2930–40.

40 Munoz-Erazo L, Rhodes JL, Marion VC, *et al*. Tertiary lymphoid structures in cancer - considerations for patient prognosis. *Cell Mol Immunol* 2020;17:570–5.

41 Sautès-Fridman C, Petitprez F, Calderaro J, *et al*. Tertiary lymphoid structures in the era of cancer immunotherapy. *Nat Rev Cancer* 2019;19:307–25.

42 Rovers KP, Wassenaar ECE, Lurvink RJ, *et al*. Pressurized intraperitoneal aerosol chemotherapy (oxaliplatin) for unresectable colorectal peritoneal metastases: a multicenter, single-arm, phase II trial (CRC-PIPAC). *Ann Surg Oncol* 2021;28:5311–26.

43 Jeong S-Y, Jeon BG, Kim J-E, *et al*. Interleukin 10 level in the peritoneal cavity is a prognostic marker for peritoneal recurrence of T4 colorectal cancer. *Sci Rep* 2021;11:9212.

44 De Vita F, Orditura M, Galizia G, *et al*. Serum interleukin-10 levels in patients with advanced gastrointestinal malignancies. *Cancer* 1999;86:1936–43.

45 Galizia G, Orditura M, Romano C, *et al*. Prognostic significance of circulating IL-10 and IL-6 serum levels in colon cancer patients undergoing surgery. *Clin Immunol* 2002;102:169–78.

46 Stanilov N, Miteva L, Deliysky T, *et al*. Advanced colorectal cancer is associated with enhanced IL-23 and IL-10 serum levels. *Lab Med* 2010;41:159–63.

47 Langenskiöld M, Holmdahl L, Falk P, *et al*. Increased TGF-beta 1 protein expression in patients with advanced colorectal cancer. *J Surg Oncol* 2008;97:409–15.

48 Bellone G, Gramigni C, Vizio B, *et al*. Abnormal expression of endoglin and its receptor complex (TGF-β1 and TGF-β receptor II) as early angiogenic switch indicator in premalignant lesions of the colon mucosa. *Int J Oncol* 2010;37:1153–65.

49 Ö K, Kemik AS, Purisa S. Transforming growth factor beta-1 in human colorectal cancer patients. *Electronic Journal of General Medicine* 2011;8:53–6.

50 Li H, van der Leun AM, Yofe I, *et al*. Dysfunctional CD8 T cells form a proliferative, dynamically regulated compartment within human melanoma. *Cell* 2019;176:e18:775–89.

51 Jin S, Guerrero-Juarez CF, Zhang L, *et al*. Inference and analysis of cell-cell communication using CellChat. *Nat Commun* 2021;12:1088.

52 Richmond J, Tuzova M, Cruikshank W, *et al*. Regulation of cellular processes by interleukin-16 in homeostasis and cancer. *J Cell Physiol* 2014;229:139–47.

53 Varn FS, Wang Y, Cheng C. A B cell-derived gene expression signature associates with an immunologically active tumor microenvironment and response to immune checkpoint blockade therapy. *Oncoimmunology* 2019;8:e1513440.

54 Hollern DP, Xu N, Thennavan A, *et al*. B cells and T follicular helper cells mediate response to checkpoint inhibitors in high mutation burden mouse models of breast cancer. *Cell* 2019;179:e21:1191–206.

55 Rogers NJ, Lechler RI. Allorecognition. *Am J Transplant* 2001;1:97–102.

56 Lee M, Heo S-H, Song IH, *et al*. Presence of tertiary lymphoid structures determines the level of tumor-infiltrating lymphocytes in primary breast cancer and metastasis. *Mod Pathol* 2019;32:70–80.

57 Jiao S, Subudhi SK, Aparicio A, *et al*. Differences in tumor microenvironment dictate T helper lineage polarization and response to immune checkpoint therapy. *Cell* 2019;179:e13:1177–90.

58 Johansson-Percival A, He B, Li Z-J, *et al*. De novo induction of intratumoral lymphoid structures and vessel normalization enhances immunotherapy in resistant tumors. *Nat Immunol* 2017;18:1207–17.